Standoff Detection and Identification of Chemical Plumes with Long Wave Hyperspectral Imaging Sensors

Dimitris Manolakis
MIT Lincoln Laboratory
244 Wood Street
Lexington, MA 02420-9185.
dmanolakis@ll.mit.edu

October 13, 2009

Abstract

Long-wave infrared (LWIR) hyperspectral imaging sensors are widely used for the detection and identification of released chemical agents in many civilian and military applications. Current hyperspectral system capabilities are limited by variation in the background clutter as opposed to the physics of photon detection. Hence, the development of statistical models for background clutter and optimum signal processing algorithms that exploit these models are essential for the design of practical systems that satisfy user's requirements. This paper describes a signal processing system for the detection and identification of released chemical agents developed at MIT Lincoln Laboratory. We discuss the underlying signal models, key detection and identification algorithms, and some areas where the signal processing community could contribute.

1 Introduction

Standoff detection of chemical warfare agents (CWAs) is necessary when physical separation is required to put people and assets outside the zone of severe damage. An important class of standoff sensors for CWAs is based on the principles of passive infrared (IR) spectroscopy. Typical standoff CWA sensors [5, 2] utilize passive imaging spectroscopy in the LWIR atmospheric window (8-13μm). The LWIR region is well suited for gas-sensing applications because of the relative

Report Documentation Page

Form Approved
OMB No. 0704-0188

1. REPORT DATE	2. REPORT TYPE	3. DATES COVERED
OCT 2009	**N/A**	**-**

4. TITLE AND SUBTITLE	5a. CONTRACT NUMBER
Standoff Detection and Identification of Chemical Plumes with Long Wave Hyperspectral Imaging Sensors	5b. GRANT NUMBER
	5c. PROGRAM ELEMENT NUMBER
6. AUTHOR(S)	5d. PROJECT NUMBER
	5e. TASK NUMBER
	5f. WORK UNIT NUMBER
7. PERFORMING ORGANIZATION NAME(S) AND ADDRESS(ES) **MIT Linclon Laboratory Lexington, MA**	8. PERFORMING ORGANIZATION REPORT NUMBER
9. SPONSORING/MONITORING AGENCY NAME(S) AND ADDRESS(ES)	10. SPONSOR/MONITOR'S ACRONYM(S)
	11. SPONSOR/MONITOR'S REPORT NUMBER(S)

12. DISTRIBUTION/AVAILABILITY STATEMENT
Approved for public release, distribution unlimited

13. SUPPLEMENTARY NOTES
See also ADB381583. RTO-MP-SET-151 Thermal Hyperspectral Imagery (Imagerie hyperspectrale thermique). Meeting Proceedings of Sensors and Electronics Panel (SET) Specialists Meeting held at the Belgian Royal Military Academy, Brussels, Belgium on 26-27 October 2009., The original document contains color images.

14. ABSTRACT

15. SUBJECT TERMS

16. SECURITY CLASSIFICATION OF:			17. LIMITATION OF ABSTRACT	18. NUMBER OF PAGES	19a. NAME OF RESPONSIBLE PERSON
a. REPORT	b. ABSTRACT	c. THIS PAGE			
unclassified	**unclassified**	**unclassified**	**SAR**	**10**	

transparency of the atmosphere at these wavelengths and the presence of unique identifying spectral signatures for a wide range of chemicals.

In this paper, we describe and demonstrate the operation of a complete automated system for the detection of chemical clouds using an LWIR imaging spectrometer. We start with the description of a physics-based signal model that provides the basis for the development of the required signal processing algorithms. Then, we provide a brief description of the signal and clutter models, detection algorithms, constant false alarm threshold selection, discrimination-identification algorithms, spatial false alarm mitigation, and experimental results using data sets collected by a Telops FIRST hyperspectral (FTIR) sensor on an acetic acid explosive release at the Dugway Proving Ground in Utah. Due to space limitations, the description of the various signal processing algorithms will be concise. More experimental results demonstrating the performance of the automated system, in the form of movies, will be shown at the conference presentation.

2 Physics-Based Radiance Signal Model

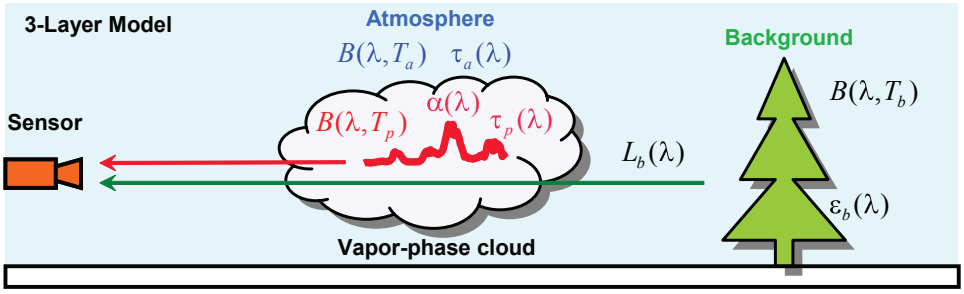

Figure 1: Three-layer plume radiance transfer model.

The physical basis for gas detection in LWIR can be explained with the following simplified model [2] (see Figure 1)

$$L_{\text{on}}(\lambda) - L_{\text{off}}(\lambda) = [1 - \tau_p(\lambda)]\,\tau_a(\lambda)\,[B(\lambda, T_p) - L_b(\lambda)] \tag{1}$$

where $L_{\text{on}}(\lambda)$ is the radiance reaching the sensor when the plume is present, $L_{\text{off}}(\lambda)$ is the radiance reaching the sensor when the plume is absent, $\tau_a(\lambda)$ is the atmospheric transmission between the chemical cloud and the sensor, $L_b(\lambda)$ the radiance of the background, $B(\lambda, T_p)$ is the Planck function evaluated at the plume temperature, and

$$\tau_p(\lambda) = \exp\left[-\alpha(\lambda) \times CL\right] \tag{2}$$

is the plume transmission function as expressed by Beer's law. We note that all quantities in (1) and (2) are functions of wavelength λ or equivalently the wavenumber ν. Natural backgrounds include low-angle sky, mountains, vegetation, urban environments, etc. All of these backgrounds emit infrared radiation in the 7-14 μm spectral region.

The function $\alpha(\lambda)$, which is known as the *absorption coefficient spectrum*, is unique for each gaseous chemical and can be used as a spectral fingerprint. The quantity CL, which is called the *concentration pathlength*, is the product of two terms: the term L, which is the length along the sensor boresight that represents the depth of the cloud, and the term C, which is the average concentration along that pathlength.

The exponential relationship between the signal of interest $\alpha(\lambda) \times CL$ and the sensor-measured differential radiance (spectral contrast) $L_{\text{on}}(\lambda) - L_{\text{off}}(\lambda)$, makes the detection and identification of gaseous chemicals a challenging problem. However, in many practical situation we can make the following assumptions:

- The plume is optically thin, that is, $CL \ll 1$. In this case, we can use the following linear approximation of Beer's law: $\tau_p(\lambda) \approx 1 - \alpha(\lambda) \times CL$.
- The emissivity of the background in the vicinity of significant gas absorption features is a smooth curve. Then, we can use the approximation $L_b(\lambda) \approx B(\lambda, T_b)$.
- We can use a local linear approximation of Planck's function about the plume temperature (valid for $|T_p - T_b|$ less than 30 degrees C).

Under these conditions, we can show that [2]

$$L_{\text{on}}(\lambda) \approx (\text{const} \times CL \times \Delta T)\tau_a(\lambda)\alpha(\lambda) + L_{\text{off}}(\lambda) \tag{3}$$

which provides the basis for the development of the detection and identification algorithms used in this paper.

3 Target and Clutter Modeling

Equation (3) is a linear relationship, which can be expressed in vector form by sampling at K wavelengths $\lambda_1, \lambda_2, \ldots, \lambda_K$, determined by the characteristics of the sensor. The results is the following linear signal model

$$\boldsymbol{x} = a\boldsymbol{s} + \boldsymbol{v} \tag{4}$$

where

$$\begin{aligned}
\boldsymbol{x} &\triangleq [L_{\text{on}}(\lambda_1) \dots L_{\text{on}}(\lambda_K)]^T \\
a &\triangleq \text{const} \times CL \times \Delta T \\
\boldsymbol{s} &\triangleq [\tau_a(\lambda_1)\alpha(\lambda_1) \dots \tau_a(\lambda_K)\alpha(\lambda_K)]^T \\
\boldsymbol{v} &\triangleq [L_{\text{off}}(\lambda_1) \dots L_{\text{off}}(\lambda_K)]^T
\end{aligned}$$

The spectral signature $\boldsymbol{s}$ is determined using measurements of $\alpha(\lambda_k)$ from high resolution spectral libraries and predicted values of $\tau_a(\lambda_k)$ obtained using the atmospheric transmission code MODTRAN.

The background clutter is modeled using a multivariate$t$-elliptically contoured distribution with density function

$$f(\boldsymbol{x}) = \frac{\Gamma\left(\frac{K+\nu}{2}\right)}{(\pi\nu)^{\frac{K}{2}}\Gamma\left(\frac{\nu}{2}\right)\sqrt{|\boldsymbol{R}|}}\left[1+\frac{1}{\nu}(\boldsymbol{x}-\boldsymbol{\mu})^T\boldsymbol{R}^{-1}(\boldsymbol{x}-\boldsymbol{\mu})\right]^{-\frac{K+\nu}{2}} \tag{5}$$

where $\Gamma(\ )$ is the Gamma function. The number of degrees of freedom ν controls the tails of the distribution: $\nu = 1$ leads to the multivariate Cauchy distribution (heavier tails), whereas as $\nu \to \infty$ the t-distribution approaches the multivariate normal distribution (lighter tails). The mean and covariance of $\boldsymbol{x}$ are given by $E(\boldsymbol{x}) = \boldsymbol{\mu}$ and $\text{Cov}(\boldsymbol{x}) = \frac{\nu}{\nu-2}\boldsymbol{R}, \nu \geq 3$, respectively. The quadratic form in (9) is distributed as an F-distribution

$$\delta^2 = \frac{1}{\nu}(\boldsymbol{x}-\boldsymbol{\mu})^T\boldsymbol{R}^{-1}(\boldsymbol{x}-\boldsymbol{\mu}) \sim F_{K,\nu} \tag{6}$$

with K and ν degrees of freedom. The value of ν controls the thickness of the distribution's tails. The estimation of these models from real data, which is illustrated in Figure 2, is discussed in [3].

4 Detection Algorithms

The signal model (4) describes how the presence of plume changes the radiance $\boldsymbol{v}$ of a background pixel. This change, which is known as radiance contrast, can be exploited to detect the presence of a CWA using statistical detection techniques. We have found out that the matched filter detector

$$y_{MF} = \frac{\boldsymbol{s}^T\hat{\boldsymbol{\Sigma}}_b^{-1}(\boldsymbol{x}-\boldsymbol{\mu}_b)}{\boldsymbol{s}^T\hat{\boldsymbol{\Sigma}}_b^{-1}\boldsymbol{s}} \tag{7}$$

and the adaptive cosine/coherence estimator (ACE)

$$y_{ACE} = \frac{[\boldsymbol{s}^T\hat{\boldsymbol{\Sigma}}_b^{-1}(\boldsymbol{x}-\boldsymbol{\mu}_b)]^2}{(\boldsymbol{s}^T\hat{\boldsymbol{\Sigma}}_b^{-1}\boldsymbol{s})[(\boldsymbol{x}-\boldsymbol{\mu}_b)^T\hat{\boldsymbol{\Sigma}}_b^{-1}(\boldsymbol{x}-\boldsymbol{\mu}_b)]} \tag{8}$$

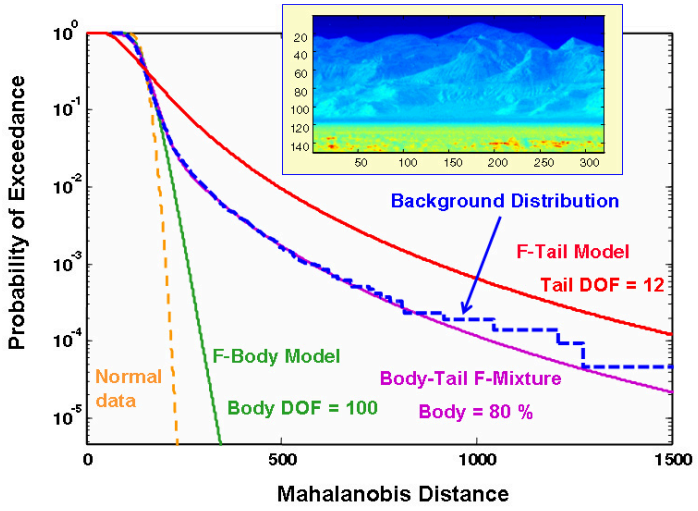

Figure 2: Modeling thermal hyperspectral backgrounds with a t-ECD relies on estimating the heavy-tail parameter by fitting a mixture of two F-distributions into the Mahalanobis distance.

provide good performance by exploiting statistical distance and angle separation in the spectral space. The quantities $\boldsymbol{\mu}_b$ and $\boldsymbol{\Sigma}_b$ are maximum likelihood estimates obtained from plume-free background clutter. More details about the application of these algorithms to hyperspectral target detection and plume detection problems can be found in [3].

5 Constant False Alarm Rate Processor

The tails of the plume-free background distribution at the output of the matched filter or ACE detectors can be modeled with sufficient accuracy using the generalized Pareto distribution (GPD) [4]. Given a sufficiently high "tail-threshold" u, the distribution $F_u(z) = \Pr(X - u \leq z | X > u)$ of excess values $z = x - u$ of x over u, converges to the GPD

$$G(z) = \begin{cases} 1 - \left(1 + \xi \frac{z}{\sigma}\right)^{-1/\xi}, & \xi \neq 0 \\ 1 - \exp(-z/\sigma), & \xi = 0 \end{cases} \tag{9}$$

which is defined for $z > 0$ and $1 + \xi z/\sigma > 0$. The quantities $\sigma > 0$ and ξ are known as scale and shape parameters, respectively. The GPD has heavy tails for $\xi > 0$, exponential tails for $\xi = 0$, and a finite upper endpoint at $-\sigma/\xi$ for $\xi < 0$.

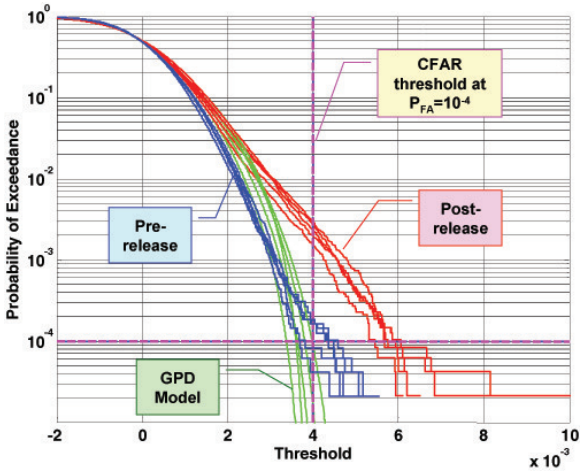

Figure 3: Illustration of GPD-based CFAR threshold selection.

The parameters of this model are estimated from the data using the method of maximum likelihood. The GPD fitted to the data can be used to approximate the tail of the unknown underlying distribution. If we denote by $\hat{\eta}$ the estimate of the threshold corresponding to a false alarm probability P_{FA}, we have

$$\hat{\eta} = u + \frac{\hat{\sigma}}{\hat{\xi}} \left[\left(\frac{\alpha}{P_{\text{FA}}} \right)^{\hat{\xi}} - 1 \right] \tag{10}$$

where u is the threshold used to estimate the parameters of the GPD and α is the fraction of samples above this threshold.

6 Discrimination and Identification Algorithms

The task of assigning a hit to one of a predetermined number of CWA classes is known as *discrimination*. When each class consists of a *single* CWA agent, discrimination is known as *identification*. The theoretical framework for detection and discrimination is the theory of statistical hypothesis testing. Therefore, detection and discrimination have some formal similarities; however, they also have some important differences.

A criterion for discrimination performance should take into consideration the importance of different CWA threats. If all threats are symmetrically treated, a meaningful figure of merit is the *probability of correct discrimination* (P_{CD}) defined by $P_{\text{CD}} = \sum_{k=1}^{p} \Pr(\text{D} = \boldsymbol{s}_k | \text{T} = \boldsymbol{s}_k)$. Using the signal model (3), the dis-

crimination problem can be stated as testing between the following p hypotheses $(k = 1, \ldots, p)$

$$H_k : \boldsymbol{x} = a_k \boldsymbol{s}_k + \boldsymbol{v} \sim N_K(a_k \boldsymbol{s}_k + \boldsymbol{\mu}_b, \boldsymbol{\Sigma}_b) \tag{11}$$

If $\{a_k, \boldsymbol{s}_k, \boldsymbol{\mu}_b, \boldsymbol{\Sigma}_b\}$ are known, the P_{CD} is minimized by the maximum likelihood classifier. This classifier computes the Mahalanobis distances of the pixel under test $\boldsymbol{x}$ from each $a_k \boldsymbol{s}_k$

$$\Delta_k^2 = (\boldsymbol{x} - \boldsymbol{\mu}_b - a_k \boldsymbol{s}_k)^T \boldsymbol{\Sigma}_b^{-1} (\boldsymbol{x} - \boldsymbol{\mu}_b - a_k \boldsymbol{s}_k) \tag{12}$$

and assigns $\boldsymbol{x}$ to the "closest" (according to Δ_k) CWA. In practice, a_k, $\boldsymbol{\mu}_b$, and $\boldsymbol{\Sigma}_b$ have to be estimated from the available data. The generalized least-squares estimate of a_k is given by

$$\hat{a}_k = \frac{\boldsymbol{s}_i^T \hat{\boldsymbol{\Sigma}}_b^{-1} (\boldsymbol{x} - \hat{\boldsymbol{\mu}}_b)}{\boldsymbol{s}_i^T \hat{\boldsymbol{\Sigma}}_b^{-1} \hat{\boldsymbol{\mu}}_b} \tag{13}$$

Substitution into (12) provides a practical discrimination algorithm. Another approach is to use the F-test developed in linear regression analysis [1].

7 Spatial Distribution of False Alarms

Figure 4 shows an example of the spatial point pattern generated by the top one percent hits at output of the matched filter for a plume-free cube and its probability distribution. It turns out that this spatial pattern follows a complete spatial randomness (CSR) model. This result and the fact that plume pixels appear in spatial clusters allows the use binary integration, "M of N" detection, or coincidence detection to improve detection performance. Binary detection is used in the automated system as part of the false alarm mitigation process.

8 Automated CWA Detection System

Figure 5 shows the basic components of the automated CWA detection/identification system. This system has been implemented in the form of a flexible MATLAB processing pipeline which allows quick experimentation with different algorithms and data sets.

To illustrate the operation of the system we use data collected by a Telops FT-IR FIRST hyperspectral sensor on an acetic acid explosive release at the Dugway Proving Ground in Utah. The specific LWIR data set used was taken on August

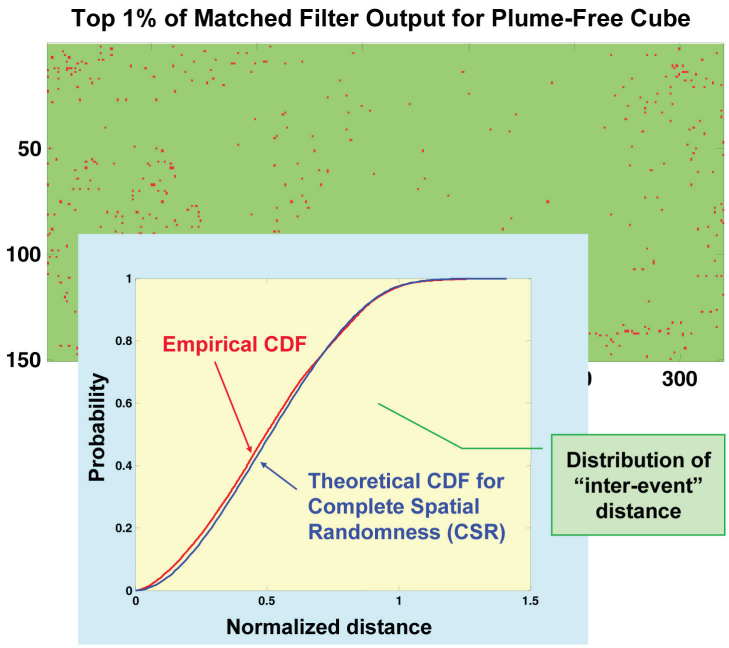

Figure 4: Extreme values of the matched filter detection statistics and the modeling of their spatial distribution with the complete spatial randomness (CSR) model.

3rd, 2006 at approximately 11:30am in the morning. The Field-of-View (FOV) of the sensor was 150 x 320 pixels, with 104 spectral bands from 8-11μm and an instantaneous FOV of 0.342 mrad. The ambient temperature at the time of the release was 29.68 degrees Celsius (302.85K), and the ambient relative humidity was 26%. In total, 43 hyperspectral cubes were captured over a span of 3.35 minutes, 22 of which were captured pre-release. There are approximately 4-5 seconds between cubes. The data used has a mountainous background scene consisting of three distinct regions: sky, mountain, and field. As an illustration, Figure 6 shows the output of the matched filter for a cube with an acetic acid plume present. Red (blue) indicates plume warmer (colder) than the background. Movies demonstrating the operation and performance of the system with various data sets will shown at the conference presentation.

9 Summary

The objective of the work reported in this paper is to develop real-time capability to detect, identify, quantify, and track the presence of chemical warfare agent threats

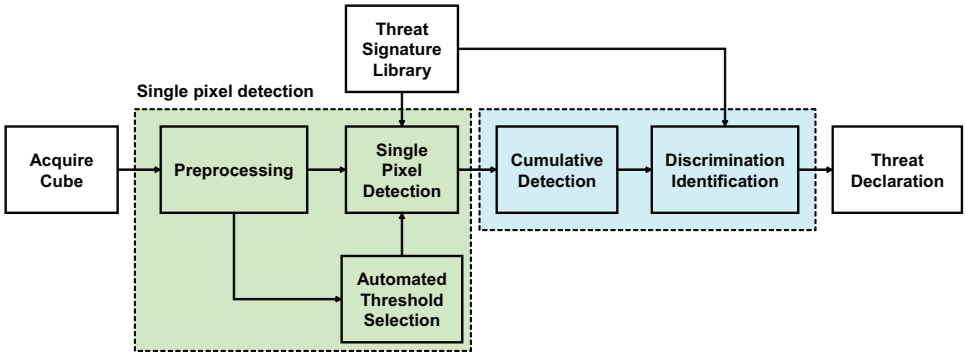

Figure 5: Automated signal processing system for hyperspectral chemical plume detection and identification.

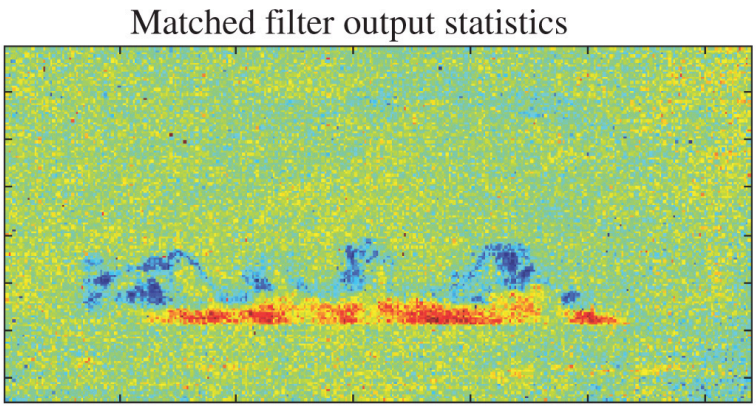

Figure 6: Example of matched filter output detection statistics.

at physiologically significant levels. We have developed and implemented in MATLAB a fully automated system for detection and identification of chemical plumes. The performance of the system has been evaluated with data collected by the US Army, Edgewood Chemical and Biological Center, for various types of chemical agents and backgrounds.

Acknowledgement

This work is sponsored by Defense Threat Reduction Agency under Air Force Contract FA8721-05-C-0002. Opinions, interpretations, conclusions, and recommendations are those of the author and not necessarily endorsed by the United

States Government. We wish to express our gratitude to Dr. Ngai Wong, Detection CAPO, JSTO-CBD, for his enthusiastic support.

References

[1] D. Manolakis. Statistical quality assessment criteria for a linear mixing model with elliptical t-distribution errors. In *Proc. SPIE 5546*, Orlando, FL, 2004. SPIE.

[2] D. Manolakis and F. D'Amico. Design and evaluation of hyperspectral algorithms for chemical warfare agent detection. In *Proc. SPIE 5995*, Orlando, FL, 2005. SPIE.

[3] D. Manolakis and G. Shaw. Detection algorithms for hyperspectral imaging application. *IEEE Signal Processing Magazine*, pages 29–43, January 2002.

[4] D. Manolakis, D. Zhang, M. Rossacci, R. Lockwood, T. Cooley, and J. Jacobson. Maintaining CFAR operation in hyperspectral target detection using extreme value distributions. In *Proc. SPIE 6565*, Orlando, FL, April 2007.

[5] A. Villemaire M. Chamberland P. Lagueux V. Farley, A. Vallières and J. Giroux. Chemical agent detection and identification with a hyperspectral imaging infrared sensor. In *Electro-Optical Remote Sensing, Detection, and Photonic Technologies and Their Applications*, pages 10.1117–12.736864. SPIE, 2007.